Spectrum of collective spontaneous emission beyond the rotating-wave approximation

Yong Li,[1] Jörg Evers,[1,2] Wei Feng,[1] and Shi-Yao Zhu[1]

[1]*Beijing Computational Science Research Center, Beijing 100084, China*
[2]*Max-Planck-Institut fur Kernphysik, Saupfercheckweg 1, 69117 Heidelberg, Germany*

The spectrum of cooperative light emission from ensembles of multilevel atoms is studied in optical vector theory and without applying the rotating-wave approximation. The effects of counter-rotating terms are included using a unitary transformation method. The spectra are analyzed and interpreted in terms of the radiative eigenmodes of the atom ensemble. We further show how the qualitative features arise from the structure of the underlying two-particle dipole-dipole interaction induced by the the vacuum field. We predict that for a suitable modification of the ensemble properties, the sign of the cooperative Lamb shift can be reversed, while still maintaining strong superradiant emission. Finally, we discuss the effects of finite detection resolution and of averaging over many realizations of the random distribution of atoms for given ensemble parameters.

I. INTRODUCTION

Spontaneous emission of atoms is not an immutable property, but a consequence of the coupling to the environment. This implies that it can be modified. One approach is to manipulate the dipole moments which effectively couple to the environment. For example, antisymmetric combinations of excited states can have vanishing dipole moments to a common ground state, effectively forming a decoherence-free subspace [1–3]. A different approach is to modify the atom's environment. A particularly interesting case arises if ensembles of atoms are considered, in which the dynamics of a particular atom is modified by the presence of the other atoms. Cooperative effects arising in the spontaneous emission from such ensembles have been intensively studied over many decades [3]. Relative to the emission of a single atom, ensembles can accelerate or slow down spontaneous decay, effects known as super- and subradiance, respectively [4]. Related to the atomic linewidth is the Lamb shift [5,6], which was named after Lamb [5] who first measured the relative shift of the $2s_{1/2}$ and $2p_{1/2}$ levels in hydrogen. The (single-atom) Lamb shift and spontaneous emission rate are the real and imaginary parts of a complex energy shift arising from the interaction of the atom with the vacuum field, which in leading order can be visualized as emission of a (virtual) photon from the atom and later reabsorption of the photon by the same atom. In the many-atom case, the emission and reabsorption of virtual photons between different atoms result in a collective Lamb shift [7–9], which is the dispersive counterpart of superradiance (subradiance). Superradiance and subradiance have been extensively studied theoretically and experimentally [7–29]. In contrast, experimental studies of the collective Lamb shift in particular are scarce. Recently, the collective Lamb shift was measured in an ensemble of nuclei embedded in a thin-film cavity probed in grazing incidence by a hard x-ray beam from a synchrotron light source [8]. In this experiment, the nuclei were prepared such that they act as ideal two-level systems, and the measurement technique allowed the cooperative decay of the nuclei to be followed over several orders of magnitude in the emitted light intensity. More recently, an experimental measurement of the cooperative Lamb shift was performed in two-dimensional atomic vapors with nanometer-scale thickness [9].

A problem in the theoretical analysis of the Lamb shift arises from the fact that the atoms can undergo transitions to higher atomic states, such that the atomic-level state space cannot be reduced as is otherwise customary in quantum optics. Nevertheless, the so-called rotating-wave approximation (RWA) is often applied to simplify the discussion. Then the atomic system can be reduced to two relevant atomic levels, such that evolutions to higher excited states are neglected [20–24]. However, studies of the collective spontaneous emission and the collective Lamb shift of N two-level atoms including the counter-rotating terms [7,25,26] somewhat surprisingly found that these terms can lead to non-negligible contributions to the spontaneous emission dynamics.

Motivated by this, recently we studied the collective spontaneous emission of a multilevel atomic ensemble including the effects of counter-rotating terms [28]. For this, we applied a unitary transformation method, which has been previously introduced [30] to include the effects of the counter-rotating terms at short time or long time scales for the case of a single or two multilevel atoms in vacuum or in other reservoirs with different spectra [31–34]. The advantages of such a unitary transformation method have been discussed in detail in Refs. [28,30]. In the previous paper [28], we in particular focused on the time evolution of the populations in the initially prepared state, as well as the total population in all excited atomic states.

Here, we complement this analysis by an investigation of the spectrum of the cooperative spontaneous decay. We first derive analytical expressions for the spectrum of emitted light for arbitrary single-atom-excitation initial states of the ensemble. Then we analyze the spectra for two initial states, the so-called standard Dicke and the timed Dicke states. A particular emphasis is put on the interpretation of the spectra in terms of radiative eigenmodes of the ensemble, which we study in detail for various parameter configurations. The combination of these results allows us to trace and interpret the evolution of the emission spectra from a single Lorentzian emission line in small ensembles to rather complicated spectra in more extended ensembles. As a main result, we find that for intermediate ensemble sizes, the sign of the cooperative Lamb shift changes its sign, while nevertheless strong superradiance is maintained. These results are then qualitatively explained in

terms of model calculations based on the dominant radiative eigenmode in ensembles of atoms, in comparison to the effects of the dipole-dipole interaction between two atoms induced by the vacuum field. Finally, we analyze the effects of finite detection resolution and averages over different realizations of the atom positions for given ensemble parameters.

II. MODEL AND HAMILTONIAN

The system we consider consists of N identical multilevel atoms interacting with the electromagnetic vacuum field, the same as that given in Ref. [28]. The total Hamiltonian of the system in minimal-coupling form reads ($\hbar = 1$)

$$H = \sum_j \sum_l \omega_l |l\rangle_{jj}\langle l| + \sum_{\mathbf{k}} \omega_{\mathbf{k}} b_{\mathbf{k}}^\dagger b_{\mathbf{k}}$$
$$+ \sum_{j,\mathbf{k}} \sum_{l,m} g_{\mathbf{k},lm} |l\rangle_{jj}\langle m| (b_{\mathbf{k}}^\dagger e^{-i\mathbf{k}\cdot\mathbf{r}_j} + \text{H.c.}), \quad (1)$$

where ω_l is the energy of the level $|l\rangle$, $b_{\mathbf{k}}$ ($b_{\mathbf{k}}^\dagger$) is the annihilation (creation) operator of the $\mathbf{k}$th-mode vacuum field of frequency $\omega_{\mathbf{k}}$ and wave vector $\mathbf{k}$ ($\equiv k\hat{k}$), $\mathbf{r}_j$ is the position of the jth atom, and

$$g_{\mathbf{k},lm} = |\omega_{lm}| d_{lm} \sqrt{\frac{1}{2\epsilon_0 \omega_{\mathbf{k}} V_{em}}} (\hat{d}_{lm} \cdot \hat{e}_{\mathbf{k}}^\perp)$$
$$:= g_{k,lm} (\hat{d}_{lm} \cdot \hat{e}_{\mathbf{k}}^\perp) \quad (2)$$

is the coupling strength. Here V_{em} is the quantization volume of the vacuum field and $\hat{e}_{\mathbf{k}}^\perp$ is the polarization direction of the $\mathbf{k}$th-mode field such that $\hat{e}_{\mathbf{k}}^\perp \cdot \mathbf{k} = 0$. Usually two polarizations for each optical wave vector should be considered; here and throughout this paper we just consider the one, $\hat{e}_{\mathbf{k}}^\perp$, since the other one normal to the dipole moment $\mathbf{d}_{lm}$ brings no contribution and thus is neglected. We have assumed that the dipole moments of all atoms are aligned, such that the dipole moment $\mathbf{d}_{lm} \equiv d_{lm}\hat{d}_{lm}$ for the transition between the levels $|l\rangle$ and $|m\rangle$ is identical for all the atoms. For the sake of simplicity, we can further assume that $g_{\mathbf{k},lm}$ is real. Note that $g_{\mathbf{k},lm} = 0$ for $l = m$, and we define the notations $\mathbf{r}_{jj'} \equiv \mathbf{r}_j - \mathbf{r}_{j'}$ and $\omega_{lm} \equiv \omega_l - \omega_m$.

As detailed in Ref. [28], after introducing a unitary transformation $U = \exp(iS)$ with

$$S = \sum_{j,\mathbf{k}} \sum_{l,m} \frac{g_{\mathbf{k},lm} \xi_{\mathbf{k},lm}}{i\omega_{\mathbf{k}}} |l\rangle_{jj}\langle m|(b_{\mathbf{k}}^\dagger e^{-i\mathbf{k}\cdot\mathbf{r}_j} - \text{H.c.}) \quad (3)$$

and $\xi_{\mathbf{k},lm} = \omega_{\mathbf{k}}/(\omega_{\mathbf{k}} + |\omega_{lm}|)$, and subtracting in addition the free-electron self-energy $E_{\text{self}} = -\sum_{j,\mathbf{k}} \sum_{l,m} (|g_{\mathbf{k},lm}|^2/\omega_{\mathbf{k}}) |l\rangle_{jj}\langle l|$, one can obtain the effective Hamiltonian

$$H^S = U^\dagger H U - E_{\text{self}}$$
$$= H_0^S + H_1 + H_{V1} + H_{V2} + O(g^2), \quad (4)$$

expanded in powers of $g_{\mathbf{k},lm}$. Here, H_0^S is the zeroth-order term equivalent to that in the first line of Eq. (1), but with the state energy ω_l replaced by $\omega_l' = \omega_l + \delta_l$. The energy shift δ_l can be interpreted as the single-atom nondynamic Lamb shift [33] for level $|l\rangle$. The first-order term of Hamiltonian (4), H_1, describes vacuum-induced transitions between the states and has the form of a Hamiltonian in the RWA even though

we did not apply the RWA to the original Hamiltonian Eq. (1). The second-order terms H_{V1} and H_{V2} in the Hamiltonian (4) arise due to virtual photon processes involving the emission and reabsorption of a photon within the same atom and between two different atoms, respectively, related to the counter-rotating terms in Eq. (1). For the exact form of H^S (4), see the Appendix.

Since the first-order term of the Hamiltonian (4), H_1, has the form of a Hamiltonian in the RWA, the system of multilevel atoms can effectively be reduced to an ensemble of two-level atoms. The residual contribution of the higher excited levels in the effective Hamiltonian (4) is of fourth order in the coupling constant and can be neglected.

III. TIME EVOLUTION FOR SINGLE-ATOM-EXCITATION STATES

A. Equations of motion

We now consider the special case of a single excitation distributed in the ensemble of N two-level atoms with the ground and first excited levels of the individual atoms denoted as $|g\rangle$ and $|e\rangle$, respectively. The ensemble ground state of H_0^S then is

$$|G,\mathbf{0}\rangle = |G\rangle|\mathbf{0}\rangle = |g_1 g_2 \cdots g_N\rangle|\mathbf{0}\rangle$$

with $|\mathbf{0}\rangle$ being the vacuum state of the electromagnetic field. The single-atom excited states of the system can be expressed as superpositions of basis states

$$|e_j\rangle := |g_1 g_2 \cdots e_j \cdots g_N\rangle \quad (j \in \{1, \ldots, N\}).$$

Further, we denote the electromagnetic field state with one photon in mode $\mathbf{k}$ by $|1_{\mathbf{k}}\rangle$.

For the dynamics of the system with initially one atomic excitation in the atoms, the single-excitation states ($|e_j,\mathbf{0}\rangle$ and $|G,1_{\mathbf{k}}\rangle$) span the relevant sub-Hilbert space. The wave function in this single-excitation case can be written in the interaction picture as

$$|\psi(t)\rangle = \sum_j \beta_j(t)|e_j,\mathbf{0}\rangle + \sum_{\mathbf{k}} \eta_{\mathbf{k}}(t)|G,1_{\mathbf{k}}\rangle. \quad (5)$$

Using the Schrödinger equation with the initial value $\eta_{\mathbf{k}}(0) = 0$ and formally integrating the equation of the time derivative of $\eta_{\mathbf{k}}(t)$ leads to

$$\eta_{\mathbf{k}}(t) = -i \sum_{j'} \frac{2\omega_{eg} g_{\mathbf{k},eg} e^{-i\mathbf{k}\cdot\mathbf{r}_{j'}}}{\omega_{\mathbf{k}} + \omega_{eg}} \int_0^t e^{-i(\omega_{eg}' - \omega_{\mathbf{k}})t'} \beta_{j'}(t') dt'.$$
$$(6)$$

Substituting this result into the equation of motion for $\beta_j(t)$, and in the Markov approximation and long time limit, one finds

$$\dot{\beta}_j(t) = -\frac{\Gamma_0}{2}\beta_j(t) - \sum_{j'(\neq j)} \frac{\Gamma_{j'}^{(j)}}{2}\beta_{j'}(t). \quad (7)$$

Here,

$$\Gamma_0 = \gamma_0 - i\frac{2\gamma_0}{\pi} \quad (8)$$

is the complex single-atom decay rate where the real part $\gamma_0 = k_{eg}^3 d_{eg}^2/(3\pi\epsilon_0)$ is the standard single-atom spontaneous

emission rate in the vector theory [35] and the term "$-\gamma_0/\pi$" ($=:L_0$) coming from the imaginary part is the single-atom dynamic Lamb shift [28]. The second term in the right side of Eq. (7), describing the vacuum-induced dipole-dipole interaction between two different atoms j and j', can be evaluated to give

$$\Gamma_{j'}^{(j)} = \sin^2 \theta_{jj'} \Gamma_{j',1}^{(j)} + \frac{(3\cos^2\theta_{jj'} - 1)}{2}\Gamma_{j',2}^{(j)}, \qquad (9)$$

where

$$\Gamma_{j',1}^{(j)} = -i\frac{3\exp(i\zeta_{jj'})}{2\zeta_{jj'}}\gamma_0 \qquad (10)$$

is proportional to the induced term in the scalar photon theory [see Eq. (A7) in Ref. [25]], and

$$\Gamma_{j',2}^{(j)} = \frac{3}{\zeta_{jj'}^3}\gamma_0[(\sin\zeta_{jj'} - \zeta_{jj'}\cos\zeta_{jj'})$$
$$+ i(1 - \cos\zeta_{jj'} - \zeta_{jj'}\sin\zeta_{jj'})] \qquad (11)$$

with $\zeta_{jj'} := k_{eg}r_{jj'} \equiv \omega_{eg}r_{jj'}/c$. Note that $\theta_{jj'}$ is the angle between $\hat{d}_{eg}$ and $\mathbf{r}_{jj'}$, and we have assumed the dipole moments of the atoms to be aligned along the z direction ($\hat{d}_{eg} = \hat{z}$).

B. Eigensystem analysis

The equations of motion (7) for the state coefficients β_j can be rewritten in matrix-vector notation as

$$\frac{d}{dt}\vec{\beta} = -\mathbf{\Gamma}\vec{\beta}, \qquad (12)$$

where $\vec{\beta} \equiv (\beta_1,\ldots,\beta_N)^{\mathrm{T}}$ and the matrix $\mathbf{\Gamma}$ has elements

$$\mathbf{\Gamma}_{jj'} = \begin{cases} \Gamma_0/2 & \text{for} \quad j = j', \\ \Gamma_{j'}^{(j)}/2 & \text{for} \quad j \neq j'. \end{cases} \qquad (13)$$

The problem of the time evolution of cooperative spontaneous emission of N atoms thus reduces to finding all (right) eigenstates (or eigenvectors, eigenmodes) $|v^{(n)}\rangle$ and complex eigenvalues λ_n of the matrix $\mathbf{\Gamma}$ [25,28,36].

After obtaining the eigenvalues and eigenvectors from the secular equation by numerical calculation, one can readily calculate the time evolution of an arbitrary initial single-atom-excitation state $|\psi(0)\rangle$. For this, the initial state is decomposed into a superposition of eigenstates $|v^{(n)}\rangle$ as

$$|\psi(0)\rangle = \sum_{n=1}^{N} C_n |v^{(n)}\rangle, \qquad (14)$$

such that its time evolution is

$$|\psi(t)\rangle = \sum_n C_n e^{-\lambda_n t} |v^{(n)}\rangle. \qquad (15)$$

If one of the C_n dominates the initial state, then the initial state $|\psi(0)\rangle$ is an approximate (exponentially decaying) eigenstate, with the real part of the related eigenvalue corresponding to the collective (half) decay rate and the imaginary part to the collective Lamb shift. Otherwise, $|\psi(0)\rangle$ is not an eigenstate, such that its time evolution is complicated since it is a superposition of different exponentially decaying components.

Note that the matrix $\mathbf{\Gamma}$ corresponding to Eq. (7) or Eq. (13) is symmetric rather than Hermitian. Consequently, the eigenstates $|v^{(n)}\rangle$ satisfy a transpose orthogonality condition rather than Hermitian orthogonality [36]. If the nth eigenstate $|v^{(n)}\rangle$ is written as $(v_1^{(n)},\ldots,v_N^{(n)})^{\mathrm{T}}$ in the single-atom-excitation basis $\{|e_j,\mathbf{0}\rangle\}$ with the jth element $v_j^{(n)} = \langle e_j,\mathbf{0}|v^{(n)}\rangle$, then $\langle u^{(n)}|$, which is defined as $(v_1^{(n)},\ldots,v_N^{(n)})$ in the same basis, is the nth (left) eigenstate of the matrix $\mathbf{\Gamma}$ with the eigenvalue λ_n. The corresponding orthogonality relation is $\sum_{j=1}^{N} v_j^{(m)} v_j^{(n)} = \delta_{mn}$ or $\langle u^{(m)}|v^{(n)}\rangle = \delta_{mn}$. Further, the coefficient C_n in Eq. (14) is determined by

$$C_n = \langle u^{(n)}|\psi(0)\rangle. \qquad (16)$$

The amplitude of the single-atom-excitation state $\beta_j(t)$ in Eq. (7) then follows as

$$\beta_j(t) = \langle e_j,\mathbf{0}|\psi(t)\rangle = \sum_{n=1}^{N} C_n v_j^{(n)} e^{-\lambda_n t}. \qquad (17)$$

IV. SPECTRUM

In a previous work [28], we have discussed the collective spontaneous emission in the present system, by considering the time-dependent population in the initial state

$$P^{(I)}(t) = |\langle\psi(0)|\psi(t)\rangle|^2, \qquad (18)$$

and the total population in all atomic excited states

$$P^{(T)}(t) = \sum_j \langle e_j,\mathbf{0}|\psi(t)\rangle\langle\psi(t)|e_j,\mathbf{0}\rangle. \qquad (19)$$

Both the Dicke state [4]

$$|D\rangle = \frac{1}{\sqrt{N}}\sum_j |e_j,\mathbf{0}\rangle \qquad (20)$$

and the timed Dicke state (also called the exciton state or single-excitation state of quasi-spin-waves) [7,14,23,27,36,37]

$$|T_{\mathbf{k}_I}\rangle = \frac{1}{\sqrt{N}}\sum_j e^{i\mathbf{k}_I\cdot\mathbf{r}_j}|e_j,\mathbf{0}\rangle \qquad (21)$$

were considered as initial states. Here, $\mathbf{k}_I$ is the wave vector of the single-photon field which prepared the state and thus defined the relative phase of the different excitation possibilities.

In this work, we focus on the spectrum of the collective spontaneous emission of the atomic ensemble. Upon spontaneous emission out of an initial single-atom-excited state such as $|D\rangle$ or $|T_{\mathbf{k}_I}\rangle$, the amplitudes of the single-photon states $|1_{\mathbf{k}}\rangle$ in the long-time limit $\eta_{\mathbf{k}}(t\to\infty)$ are given by

$$\eta_{\mathbf{k}}(\infty) = -i\sum_j \frac{2\omega_{eg}g_{\mathbf{k},eg}e^{-i\mathbf{k}\cdot\mathbf{r}_j}}{\omega_{\mathbf{k}} + \omega_{eg}}\int_0^\infty e^{i(\omega_{\mathbf{k}}-\omega'_{eg})t'}\beta_j(t')dt'$$

$$\approx -i\sum_j\sum_n \frac{2\omega_{eg}g_{\mathbf{k},eg}e^{-i\mathbf{k}\cdot\mathbf{r}_j}}{\omega_{\mathbf{k}} + \omega_{eg}}\frac{C_n v_j^{(n)}}{\lambda_n + i(\omega_{eg} - \omega_{\mathbf{k}})}$$

according to Eqs. (6) and (17). Here we have approximated ω'_{eg} by ω_{eg} in the exponential function as it only leads to a shift which is identical for each atom.

Let us first consider a detector positioned at $\mathbf{R}$, far away from the center of the atomic ensemble with position $\mathbf{0}$. Thus, $|\mathbf{R}| \equiv R$ is much larger than the resonant optical wavelength and the dimensions of the atomic ensemble. The electric field to be detected in this far-field position at time t is ($\hbar = 1$)

$$\langle G, \mathbf{0}|E^{(+)}(\mathbf{R}, t) \sum_{\mathbf{k}} \eta_{\mathbf{k}}(t)|G, 1_{\mathbf{k}}\rangle$$

$$= \sum_{\mathbf{k}} \sqrt{\frac{\omega_{\mathbf{k}}}{2\epsilon_0 V_{em}}} \hat{e}_{\mathbf{k}}^{\perp} e^{i(\mathbf{k}\cdot\mathbf{R}-\omega_k t)} \eta_{\mathbf{k}}(\infty)$$

$$:= \int d\omega_k e^{-i\omega_k t} \mathbf{B}_{\mathbf{R}}(\omega_k), \qquad (22)$$

where

$$\mathbf{B}_{\mathbf{R}}(\omega_k) = \frac{-i\omega_{eg}^2 d_{eg}}{(2\pi)^3 c^3 \epsilon_0} \frac{\omega_k^2}{\omega_k + \omega_{eg}} \sum_{j,n} \frac{C_n \nu_j^{(n)}}{\lambda_n + i(\omega_{eg} - \omega_k)}$$

$$\times \int d\Omega_{\mathbf{k}} \hat{e}_{\mathbf{k}}^{\perp}(\hat{d}_{eg} \cdot \hat{e}_{\mathbf{k}}^{\perp}) e^{i\mathbf{k}\cdot(\mathbf{R}-\mathbf{r}_j)}. \qquad (23)$$

Then the spectrum for the detector at position $\mathbf{R}$ is given by Refs. [32,35]

$$S_{\mathbf{R}}(\omega_k) = |\mathbf{B}_{\mathbf{R}}(\omega_k)|^2. \qquad (24)$$

The integration of $\mathbf{B}_{\mathbf{R}}(\omega_k)$ in Eq. (23) over all emission directions can be performed using [1]

$$\int d\Omega_{\mathbf{k}} \hat{e}_{\mathbf{k}}^{\perp}(\hat{d}_{eg} \cdot \hat{e}_{\mathbf{k}}^{\perp}) e^{i\mathbf{k}\cdot(\mathbf{R}-\mathbf{r}_j)}$$

$$= \int d\Omega_{\mathbf{k}}[\hat{d}_{eg} - \hat{k}(\hat{k} \cdot \hat{d}_{eg})] e^{i\mathbf{k}\cdot\mathbf{R}^{(j)}}$$

$$\approx [\hat{d}_{eg} - \hat{R}^{(j)}(\hat{R}^{(j)} \cdot \hat{d}_{eg})] \int d\Omega_{\mathbf{k}} e^{i\mathbf{k}\cdot\mathbf{R}^{(j)}}$$

$$\approx \frac{2\pi i}{kR} [\hat{R} \times (\hat{R} \times \hat{d}_{eg})] (e^{ikR^{(j)}} - e^{-ikR^{(j)}}). \qquad (25)$$

Here, $\mathbf{R}^{(j)} := \mathbf{R} - \mathbf{r}_j := R^{(j)}\hat{R}^{(j)}$ with $R^{(j)} \approx R - \mathbf{R} \cdot \mathbf{r}_j$, and we have used $\int d\Omega_{\mathbf{k}} e^{i\mathbf{k}\cdot\mathbf{r}} = -2\pi i(e^{ikr} - e^{-ikr})/(kr)$. In the third line we have used the approximation that the optical modes whose wave vectors are not parallel to $\mathbf{R}^{(j)}$ lead to negligible contributions. Thus, we replaced $\hat{k}$ by $\hat{R}^{(j)}$ and further used $R^{(j)} \approx R$ and $\hat{R}^{(j)} \approx \hat{R}$ in the last step, except for the phases in the exponential function. As noted before, we consider a single polarization and neglected the second one normal to the $\hat{d}_{eg}$ in the first line of Eq. (25). Alternatively, we can consider both polarizations by replacing $d\Omega_{\mathbf{k}}\hat{e}_{\mathbf{k}}^{\perp}(\hat{d}_{eg} \cdot \hat{e}_{\mathbf{k}}^{\perp})$ with $\sum_{s=1,2} d\Omega_{\mathbf{k}}\hat{e}_{\mathbf{k}}^{(s)}(\hat{d}_{eg} \cdot \hat{e}_{\mathbf{k}}^{(s)})$, which will lead to the same results. Note that in the last line of Eq. (25), the terms $e^{ikR^{(j)}}$ and $e^{-ikR^{(j)}}$ represent the outward and incoming waves, respectively, and we will therefore neglect the latter [32,35] by imposing suitable boundary conditions.

Combining all steps, we obtain for the emission-angle-resolved spectrum

$$S_{\mathbf{R}}(\omega_k) \propto [\hat{R} \times (\hat{R} \times \hat{d}_{eg})]^2 \left| \sum_{j,n} \frac{C_n \nu_j^{(n)} \exp[ikR^{(j)}]}{\lambda_n + i(\omega_{eg} - \omega_k)} \right|^2. \qquad (26)$$

In Eq. (26), the factor $\hat{R} \times (\hat{R} \times \hat{d}_{eg})$ is related to the direction of the detector. The coefficient C_n represents the projection

of the initial state on the nth eigenstate, and $\nu_j^{(n)} = \langle e_j, \mathbf{0}|\nu^{(n)}\rangle$ is the product of the nth eigenstate and the jth single-atom excited state $|e_j, \mathbf{0}\rangle$. The denominator $\lambda_n + i(\omega_{eg} - \omega_k)$ shows the collective decay rate and collective Lamb shift for the nth eigenstate. The factor $\exp[ikR^{(j)}]$ denotes the phase acquired by the light traveling from the position of the jth atom to the detector position. Further, the total spectrum integrated over all emission directions is given by

$$S(\omega_k) = \int d\Omega_{\mathbf{R}} S_{\mathbf{R}}(\omega_k) = \sum_{j,j'} f_j(k) f_{j'}^*(k) T_{jj'}(k), \qquad (27)$$

where $f_j(k) = \sum_n C_n \nu_j^{(n)}/[\lambda_n + i(\omega_{eg} - \omega_{\mathbf{k}})]$ and

$$T_{jj'}(k) = \int d\Omega_{\mathbf{R}}[\hat{R} \times (\hat{R} \times \hat{d}_{eg})]^2 e^{ik\mathbf{R}\cdot\mathbf{r}_{jj'}} \qquad (28)$$

evaluates to $8\pi/3$ for $j = j'$ and to

$$\frac{4\pi \sin kr_{jj'}}{kr_{jj'}} \sin^2 \theta_{jj'}$$

$$+ \frac{4\pi(\sin kr_{jj'} - kr_{jj'} \cos kr_{jj'})}{(kr_{jj'})^3}(3\cos^2 \theta_{jj'} - 1) \qquad (29)$$

for $j \neq j'$. As noted before, $\theta_{jj'}$ is the angle between $\mathbf{r}_{jj'}$ and $\hat{d}_{eg}$.

In the following numerical calculation, we will calculate the total spectrum $S(\omega)$ for the initial Dicke state $|D\rangle$ and the timed Dicke state $|T_{\mathbf{k}_I}\rangle$ with $\mathbf{k}_I = k_{eg}\hat{k}_I = k_{eg}\hat{x}$ (and $\hat{d}_{eg} \equiv \hat{z}$).

V. NUMERICAL RESULTS FOR THE SPECTRA

A. The spectrum for N atoms in a sphere

First, we consider the spectrum of the collective spontaneous emission for an initial Dicke state $|D\rangle$ with $N = 6000$ atoms randomly distributed in spheres with different radii R_a. Results are shown in Fig. 1. Figure 1(a1) shows a volume with dimensions much smaller than the wavelength of the emitted radiation. It can be seen that the spectrum essentially consists of a single peak, which is shifted substantially towards lower frequencies compared to the single-atom resonance frequency, and which has a width of order $N\gamma_0$. These are the results expected for the well-known case of standard Dicke superradiance. In this case, the initial Dicke state is approximately a radiative eigenstate of the system. The real part of the eigenvalue of this eigenmode is about $N\gamma_0/2$ (half of the spectral width), indicating accelerated collective decay. Its imaginary part indicates a negative collective Lamb shift. Note that we have neglected the single-atom Lamb shift during all of the numerical calculations, such that only the collective Lamb shifts are shown.

Next, in Fig. 1(a2), a larger ensemble volume is considered. While the spectrum still is dominated by a single superradiantly broadened peak, the cooperative Lamb shift has reversed its sign, such that the peak is shifted towards higher frequencies compared to the single-atom resonance frequency. On increasing the volume further [$R_a = 2\lambda$ in Fig. 1(a3)], again a single peak is found, but with reduced (positive) cooperative Lamb shift and superradiance. Finally, at $R_a = 5\lambda$ in Fig. 1(a4), the spectrum starts to decompose into multiple lines, which however in total still approximately lead
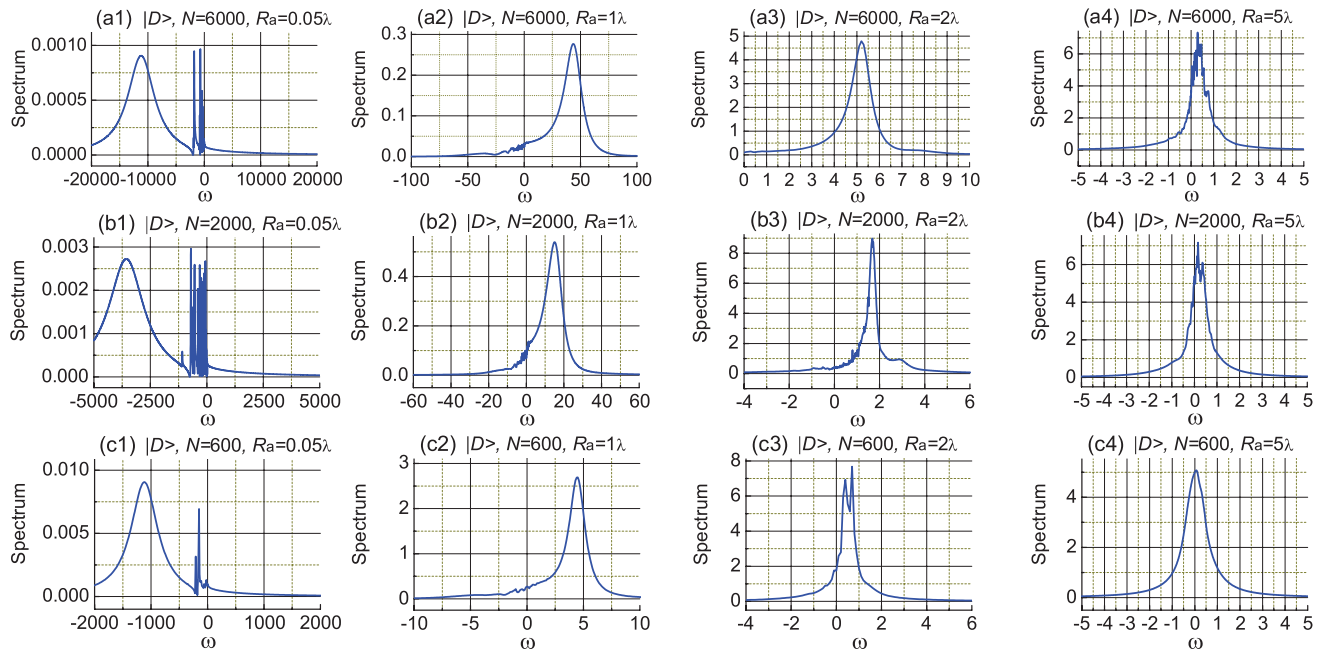
FIG. 1. (Color online) Total emission spectrum $S(\omega + \omega_{eg})$ (in arbitrary units) against ω (in units of γ_0) for (a1)–(a4) $N = 6000$, (b1)–(b4) $N = 2000$, and (c1)–(c4) $N = 600$ atoms for the initial Dicke state $|D\rangle$. The atoms are randomly placed in a sphere with radius (a1), (b1), (c1) $R_a = 0.05\lambda$, (a2), (b2), (c2) $R_a = 1\lambda$, (a3), (b3), (c3) $R_a = 2\lambda$, and (a4), (b4), (c4) $R_a = 5\lambda$.

to a single peak in the spectrum. In this case, however, the width of the total main peak is less than γ_0, indicating subradiance. In the limit of low volume density, starting from about $\lesssim 1$ atom/λ^3, the spectrum reduces to that of a single atom without a collective Lamb shift and with single-atom decay rate γ_0.

Next, we repeat the analysis for the initial state $|T_{\mathbf{k}_I}\rangle \equiv |T\rangle$ (with $\mathbf{k}_I = k_{eg}\hat{k}_I = k_{eg}\hat{x}$). When the atoms are randomly distributed in a sphere with radius much smaller than the typical wavelength, the spectrum of $|T\rangle$ [Fig. 2(a1)] is similar to that of $|D\rangle$ [Fig. 1(a1)], with enhanced collective decay rate and large negative collective Lamb shift. The reason for this is that in the limit of small ensemble volume, $|T\rangle$ coincides with $|D\rangle$.

As the radius increases, the cooperative Lamb shift and the superradiant line broadening decrease, as shown in Fig. 2(a2). Eventually, a second major peak appears, which has a positive cooperative Lamb shift; see the case of $R_a = 2\lambda$ in Fig. 2(a3). Thus, the spectrum cannot be interpreted as arising from a single radiative eigenmode, but rather has two contributions with opposite cooperative Lamb shifts. As the radius increases further, the two peaks of the spectrum become closer and closer and finally are reduced to one peak centered at 0. Note that in this case the collective decay rate is still larger than that in the single-atom case; see Fig. 2(a4). When the radius is large enough, the spectrum will be reduced to that of independent atoms. However, in comparison to the case of $|D\rangle$, we note that initial $|T\rangle$ states require larger volumes or smaller densities to reduce to the single-atom case.

In order to interpret our findings, in the second and third rows of Fig. 1 (Fig. 2), we show corresponding results with $N = 2000$ in the second row and $N = 600$ in the third. The separate variation of size and atom number allows effects of the ensemble geometry and the atom number density to be distinguished.

First, we analyze the spectra for different N, but with fixed volume and geometry. As can be seen from Figs. 1(a1), 1(b1), and 1(c1) for $R_a = 0.05\lambda$ and initial $|D\rangle$ state, in all cases, a single peak with negative cooperative Lamb shift and strong superradiance proportional to N is obtained. Only the magnitude of the shift and the line broadening decrease with N. For intermediate radii $R_a = 1\lambda$ [Figs. 1(a2), 1(b2), and 1(c2)] or $R_a = 2\lambda$ [Figs. 1(a3), 1(b3), and 1(c3)], again the main spectral features are qualitatively similar for different N. In all cases, a single main peak dominates, which has a positive collective Lamb shift proportional to N. Also, the linewidth increases as N increases. There are, however, some differences in the collective decay rates in these two intermediate cases. In the former case, the collective decay rate is always larger than γ_0 (superradiance) for $N \sim 10^3$. In the latter case, it is less than γ_0 (subradiance) for $N = 600$ and $N = 2000$, but larger than γ_0 for $N = 6000$. Finally, for radius $R_a = 5\lambda$ shown in Figs. 1(a4), 1(b4), and 1(c4), the spectrum for $|D\rangle$ resembles the single-atom case, but with a small positive collective Lamb shift and a subradiance [see $N = 6000$ and $N = 2000$ in Figs. 1(a4) and 1(b4)]. Note, however, that this applies only to $N \sim 10^3$. When N becomes large enough, superradiance will appear for this geometry.

We now turn to initial state $|T\rangle$. Comparing the different rows of Fig. 2, as for the $|D\rangle$ state, we find that the results remain qualitatively similar for the different numbers of atoms, with main features as discussed in the case of $N = 6000$. Quantitatively, the magnitudes of the cooperative Lamb shift and of the linewidth decrease with N. For the largest volume with smaller $N = 600$ in Fig. 2(c4), the two peaks found for larger atom number already have merged into a single line.

Note that next to the main features discussed so far, there are narrow spikes in the discussed spectra. These will be explained later in Sec. V D.
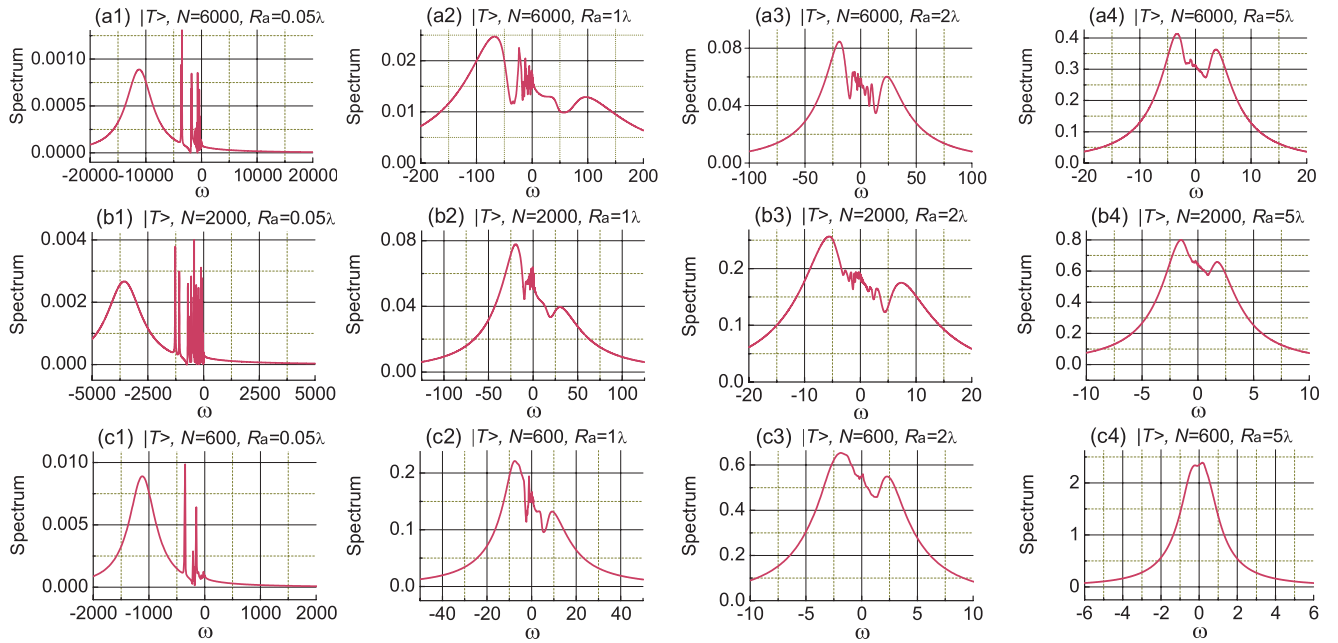
FIG. 2. (Color online) Total emission spectrum $S(\omega + \omega_{eg})$ (in arbitrary units) against ω (in units of γ_0) for (a1)–(a4) $N = 6000$, (b1)–(b4) $N = 2000$, and (c1)–(c4) $N = 600$ atoms for the initial timed Dicke state $|T\rangle$ $(:= |T_{\mathbf{k}_I}\rangle)$ with $\mathbf{k}_I = k_{eg}\hat{k}_I = k_{eg}\hat{x}$. The atoms are randomly placed in a sphere with radius (a1), (b1), (c1) $R_a = 0.05\lambda$, (a2), (b2), (c2) $R_a = 1\lambda$, (a3), (b3), (c3) $R_a = 2\lambda$, and (a4), (b4), (c4) $R_a = 5\lambda$.

B. Radiative eigenmodes

The above phenomena in the spectra for the initial Dicke state $|D\rangle$ can be understood from the radiative eigenmode structure for the given ensemble. It manifests itself in the distribution of coefficients C_n which contribute to the initial state. As can be seen from Eq. (26), the coefficient C_n reflects the importance of the nth eigenmode to initial-state decay, and also to the spectrum of spontaneous emission of the initial state. If the absolute value of one of the C_n's is much larger than that of all others, then only this mode dominates the dynamics, and the spectra are dominated by only one peak. If there are many C_n's whose absolute values are of the same order, then the spectrum receives contributions of many eigenmodes, and in general is rather complicated. Each of the eigenmodes contributes with thereal and imaginary parts of its eigenvalues to the cooperative shift and line broadening. In Figs. 3 and 4, we show the magnitude $|C_n^2|$ as a function of the real and the imaginary parts of the corresponding eigenvalue, respectively.

When the ensemble radius is small as in Figs. 3(a), 3(b), 4(a), and 4(b), then only one of the eigenstates dominates for the initial state $|D\rangle$. This can be seen from the fact that a single

dot [marked as (i) in Figs. 3(a), 3(b), 4(a), and 4(b)] appears in the figures with large $|C_n^2|$, while the dots belonging to all other modes have negligible contribution. This means that $|D\rangle$ is approximately a radiative eigenstate of the ensemble in this case. Thus, the spectrum mainly consists of a single Lorentzian peak with a Lamb shift corresponding to the imaginary part and superradiance corresponding to the real part of the eigenvalue of the dominating mode.

As already seen from the spectra, we find that with increasing ensemble size, a single mode remains dominant, but the imaginary part of the eigenvalue increases until it turns positive, while the real part remains much larger than 1, indicating superradiance; see Figs. 3(b) and 4(b).

With intermediate radius $R_a = 2\lambda$, there are three eigenstates which contribute most to the spectrum; see the dots (i), (ii), and (iii) in Figs. 3(c) and 4(c). All of their imaginary parts are about $1.8\gamma_0$ and all of their real parts are about $0.25\gamma_0$. Thus, in the spectrum, they can be expected to overlap, and to lead to a combined peak with cooperative Lamb shift $1.8\gamma_0$ and width $0.5\gamma_0$ (corresponding to subradiance). This prediction is in agreement with the spectrum in Fig. 1(b3).
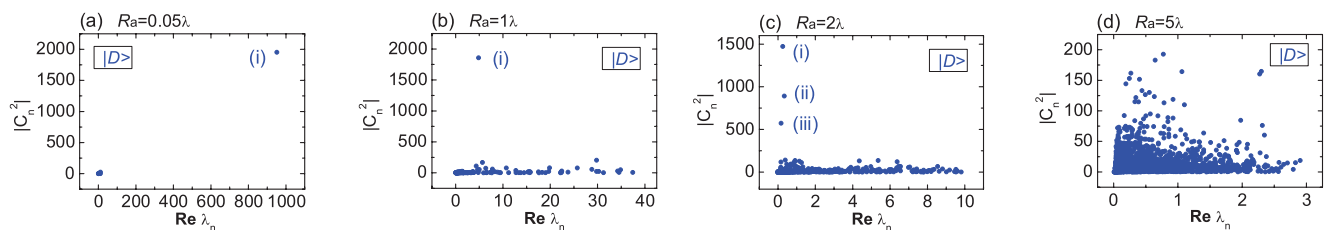

FIG. 3. (Color online) Magnitude of the contribution of the different radiative eigenmodes (in arbitrary units) as a function of the real part of their corresponding eigenvalue (in units of γ_0). Results are shown for an initial standard Dicke state $|D\rangle$ for different ensemble radii with number of atoms $N = 2000$, according to the second row of Fig. 1.
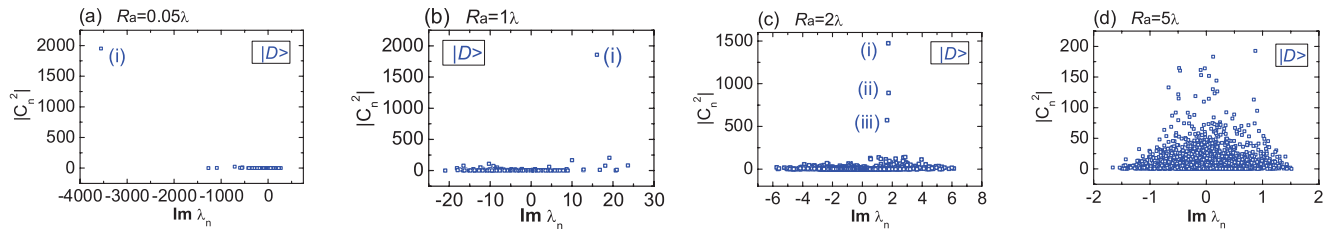
FIG. 4. (Color online) Magnitude of the contribution of the different radiative eigenmodes (in arbitrary units) as a function of the imaginary part of their corresponding eigenvalue (in units of γ_0). Results are shown for an initial standard Dicke state $|D\rangle$ for different ensemble radii with number of atoms $N = 2000$, according to the second row of Fig. 1.

When the radius of the atomic ensemble is large [e.g., larger than 5λ as given in Figs. 3(d) and 4(d)], there are many eigenstates having important contributions with average real parts of their eigenvalues of about $\gamma_0/2$, which corresponds to the single-atom case. The average of the imaginary parts of the eigenvalues is about 0, which indicates a vanishing cooperative Lamb shift. This explains why the spontaneous emission of the initial Dicke state $|D\rangle$ in this case reduces to the single-atom case. In this case, the initial state does not correspond to any of the radiative eigenmodes of the ensemble at all.

For the initial state $|T\rangle$, the small-volume cases [see Figs. 5(a) and 6(a)] are again similar to the case with initial state $|D\rangle$. When the volume increases [Figs. 5(b)–5(d) and 6(b)–6(d)], usually there are many eigenstates with non-negligible contributions. But in contrast to the other initial state $|D\rangle$, here, some of them have large positive imaginary parts of their eigenvalues, while others have large negative imaginary parts of their eigenvalues. This explains why the spectrum approximately consists of two peaks with opposite signs of the cooperative Lamb shift. Note, however, that each of these peaks consists of many different eigenmodes, which appear as one peak, as they overlap in the spectrum. When the volume is large, the imaginary parts of all eigenvalues are close to zero, such that the spectrum again appears as a single peak; see Fig. 2(c4).

It is interesting to note that for the intermediate-volume cases as in Fig. 2(b3), the two peaks in the spectrum are centered at about $-6\gamma_0$ and $7\gamma_0$, respectively, which appears inconsistent with the fact that the corresponding imaginary parts of the relevant eigenmodes are in the range $(-6,6)$. This effect results from interference between different eigenstates.

C. Interpretation of the spectra

Next, we show that the results found in the previous sections qualitatively can be understood already from the vacuum-induced dipole-dipole interaction between two particles. For this, we focus on cases in which the spectrum is dominated by a single eigenmode, and thus restrict our analysis to the mode with the largest eigenvalue. In the following, we denote this mode as the dominant mode. We evaluate this dominating eigenvalue for different cubic volumes with side length from 0.05λ up to about 2λ, and for $N = 100$ to $N = 600$ atoms. For each configuration, we calculate 25 different realizations in order to estimate the effect of the random placement of the atoms in the volume.

As a first step, we averaged over the 25 realizations for each size and atom number, and plotted the obtained real and imaginary parts of the eigenvalues against the number of atoms; see Fig. 7. In the considered parameter range, the eigenvalues depend linearly on the number of atoms, as expected for the usual Dicke superradiance. The smaller the volume is, the larger is the corresponding real part of the eigenvalue, indicating stronger superradiance. But for the imaginary part of the eigenvalue, it can be seen that starting from a certain ensemble size, the cooperative Lamb shift evolves from a large negative value to a positive value with increasing ensemble size. This clearly resembles the results found in Figs. 1 and 2. We further analyzed this analogy by plotting the imaginary part of the dominant eigenvalue for $N = 600$ atoms as a function of the ensemble size, as shown in Fig. 8(a). Comparing this result with the vacuum-induced dipole-dipole shift for two interacting two-level atoms averaged over all orientations shown in Fig. 8(b), it can be seen that the qualitative shapes of the results in (a) and (b) are similar. We can thus trace back the fact that with increasing volume size the cooperative Lamb shift changes its sign to the distance dependence of the underlying interparticle interaction induced by the vacuum. Note that the dependence on the size of the volume in Fig. 8(a) does not exactly correspond to the distance between the two atoms in Fig. 8(b). Rather,
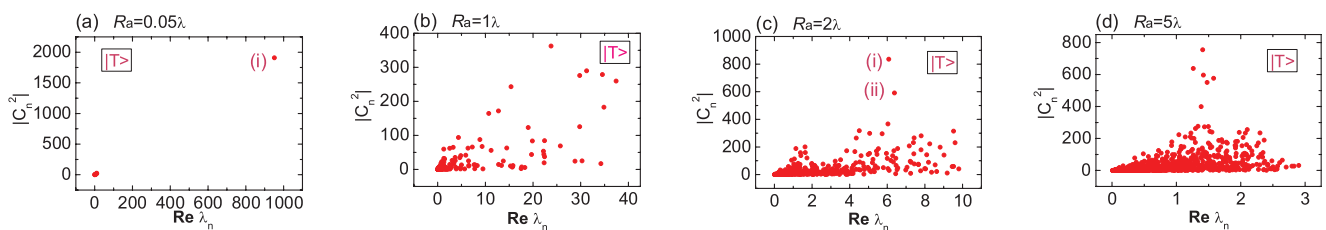

FIG. 5. (Color online) Magnitude of the contribution of the different radiative eigenmodes (in arbitrary units) as a function of the real part of their corresponding eigenvalue (in units of γ_0). Results are shown for the initial timed Dicke state $|T\rangle$ for different ensemble radii with number of atoms $N = 2000$, according to the second row of Fig. 2.
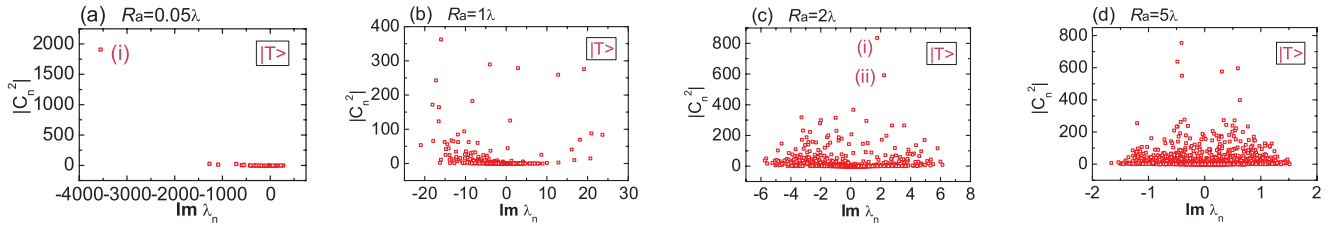
FIG. 6. (Color online) Magnitude of the contribution of the different radiative eigenmodes (in arbitrary units) as a function of the imaginary part of their corresponding eigenvalue (in units of γ_0). Results are shown for the initial timed Dicke state $|T\rangle$ for different ensemble radii with number of atoms $N = 2000$, according to the second row of Fig. 2.

each volume size corresponds to an effective distance which dominates the interaction shift. We would like to remark that a similar phenomenon of oscillating shifts was observed in the recent experiment [9] (see Fig. 4 in this reference). However, in the experiment, the shift always remained negative, while our results show the possibility of a sign change. The difference could be due to the different geometry, or to the fact that we focus on the dominant eigenmode only.

Figure 8(a) further shows that towards larger volume sizes, the oscillations of the imaginary part with the size of the volume cease, while they persist for two atoms in Fig. 8(b). This can be understood from Fig. 9(a), which again shows the imaginary part of the eigenvalue against the size of the volume. But in contrast to Fig. 7, here the results for each of the 25 realizations of the atom positions are shown separately. For small volume sizes, each of the different realizations leads to a similar cooperative Lamb shift. But from a certain

volume size on, different branches for the imaginary part become visible. These occur since, for a given size and number of atoms, the exact placement of the atoms decides whether the system has a positive or a negative cooperative Lamb shift. Interestingly, despite the fact that the atoms are placed randomly, the spectrum of possible imaginary parts is not continuous, but decomposes into a small set of discrete values. With increasing volume size, more and more of such branches appear, which eventually merge into each other. The appearance of different branches with opposite sign explain why the imaginary part in Fig. 8(a) stops oscillating from a certain system size onwards. The average performed to obtain the results of Fig. 8(a) encompasses different branches with opposite signs of the cooperative Lamb shift, which together lead to a small and approximately constant average.

As the final step, we relate the different cooperative Lamb shift branches found in Fig. 9(a) to the corresponding decay rates. Figure 9(b) shows that the decay rate and the Lamb shift
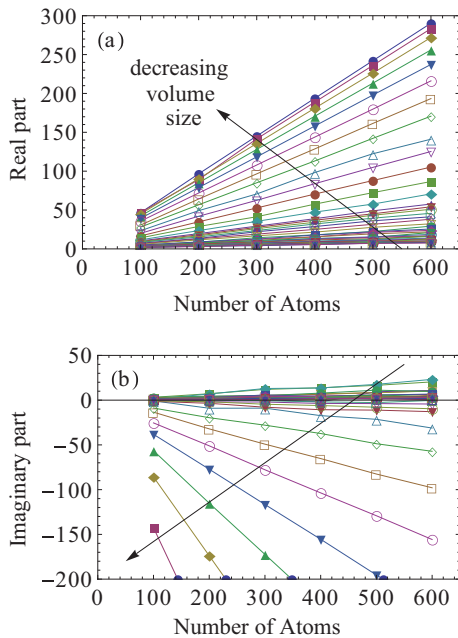

FIG. 7. (Color online) Real and imaginary parts of the eigenvalue (in units of γ_0) of the dominant eigenmode as a function of the number of atoms in the volume. The different lines show side lengths of the cubic ensemble volume ranging from 0.05λ up to 2λ. The arrow points in the direction of decreasing ensemble size. Each point is obtained by averaging over 25 different realizations of the random atom placement in the given volume.
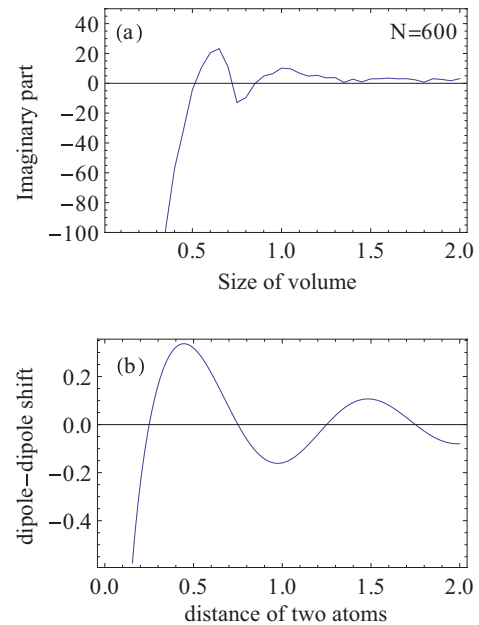

FIG. 8. (Color online) (a) Plot of the imaginary part of the eigenvalue (in units of γ_0) of the dominant eigenmode for $N = 600$ against the ensemble size (in units of λ). Each point is obtained by averaging over 25 different realizations of the random atom placement in the given volume. (b) Level shift induced by the dipole-dipole interaction for two two-level atoms as a function of the interatomic distance.
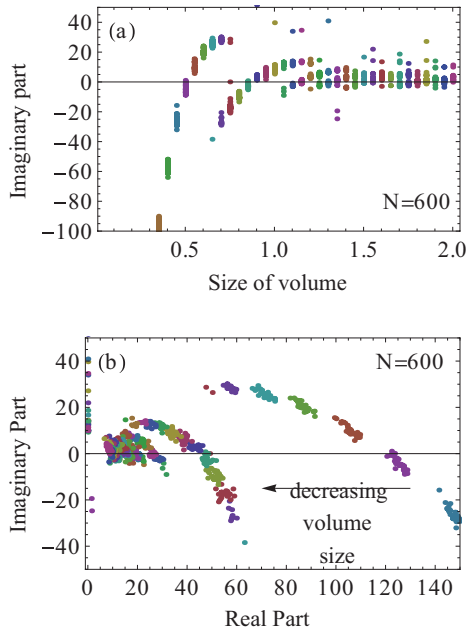
FIG. 9. (Color online) (a) Imaginary part of the eigenvalue (in units of γ_0) of the dominant eigenmode VS the size of the volume (in units of λ) for $N = 600$ atoms. (b) Imaginary part against the real part of the eigenvalue (in units of γ_0) for $N = 600$ atoms for different volume sizes. The arrow indicates the direction of decreasing size. In contrast to Fig. 7, here the result of each of the 25 realizations is shown separately, such that there is a set of points for each volume size.

of the different branches are indeed linked. The first branch on the right-hand side for small volume sizes starts with large superradiance and strong negative cooperative Lamb shift. With increasing volume size, the Lamb shift reverses its sign, and the superradiance is reduced. The second branch has a qualitatively similar shape and dependence on the volume size, and sets in at real parts of about $60\gamma_0$. Towards larger volume sizes, a multitude of branches contributes, which however have similar small real and imaginary parts of the eigenvalues, such that they appear as a single line in the spectrum.

In summary, we thus showed that the main spectral features found for the cooperative emission of smaller ensembles of atoms can be explained by considering the dominant eigenvalue only. In this case, the emission spectrum essentially consists of a single spectral line, which allows easy determination of the effective cooperative Lamb shift and cooperative decay rate. Furthermore, part of the results can qualitatively be understood from the properties of the vacuum-induced dipole-dipole interaction between two particles. This is consistent with the fact that we found a strong dependence of the qualitative properties of the emission spectra on the sample geometry, which translates into an effective distance in the two-atom system.

D. Convolution spectrum and average spectrum

In the spectra shown in Figs. 1 and 2, next to the main spectral peaks, a number of narrow spikes are visible. In the following, we analyze their significance. First, we analyze to what extent the spikes depend on the microscopic realization
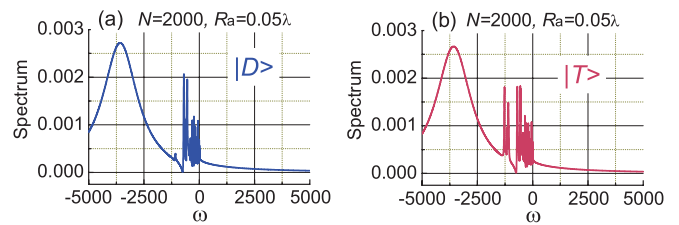

FIG. 10. (Color online) Emission spectrum $S(\omega + \omega_{eg})$ (in arbitrary units, against ω in units of γ_0) averaged over 100 realizations of the random atom placement in a sphere with $R_a = 0.05\lambda$ for initial state (a) $|D\rangle$ and (b) $|T\rangle$.

of our ensemble. For all calculations, we randomly place a certain number of atoms in a given volume. Therefore, the results in principle could vary from realization to realization, as the atoms are placed at different positions. In an experiment it is likely that results of multiple measurements would have to be averaged, such that only structures could be observed which persist under such an ensemble average. We therefore calculated the average spectrum over 100 realizations of random atom distributions. The result is shown in Fig. 10, and it can be seen that the results are very similar to the single realizations reported in Figs. 1 and 2. This shows that our numerical calculations are stable in the sense that the spikes are not an artifact of the specific atom distribution.

Next, we consider the finite detector resolution. Each of the spikes corresponds to a radiative eigenmode of the system, and one way of judging the significance is by the area covered by the respective spike in the spectrum. If a mode has very low decay rate, then it leads to a structure with low width in the spectrum, which can appear prominent even if the total weight of the structure is low.

Thus, we convolute the spectra via

$$S_{\text{con}}(\omega) = \int d\Omega S(\omega) F(\Omega - \omega), \qquad (30)$$

where $F(\omega) = \exp[-\omega^2/(4\sigma^2)]/\sqrt{2\pi}$ with σ the half-width of the convolution function. This width corresponds to the finite frequency resolution of the detection in an experiment. Figure 11 shows examples with $\sigma = 10$ and $\sigma = 100$, respectively. It can be seen that the narrow spikes disappear, such that the underlying structure becomes visible.
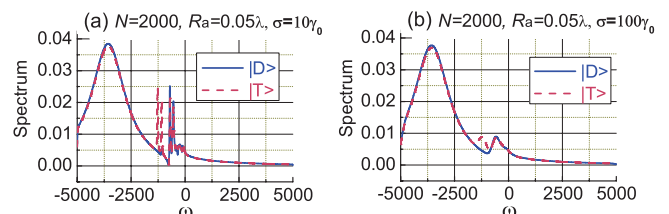

FIG. 11. (Color online) Emission spectrum $S_{\text{con}}(\omega + \omega_{eg})$ (in arbitrary units, against ω in units of γ_0) convoluted with a finite detector resolution for $N = 2000$ atoms in a sphere with $R_a = 0.05\lambda$ for initial states $|D\rangle$ and $|T\rangle$. The convolution width is (a) $\sigma = 10\gamma_0$ and (b) $\sigma = 100\gamma_0$.

VI. CONCLUSION

In conclusion, we investigated the spectrum of collective spontaneous emission for *N multilevel* atoms in vacuum. A particular unitary transformation has been used to include the counter-rotating terms in our analysis. Following the unitary transformation method, the system Hamiltonian assumes the simple RWA form for *N two-level* atoms, even though the RWA was not applied, and even though multilevel atoms are considered. We focused on the case with only one excitation initially in the atomic ensemble. The decay dynamics can then be studied by finding all eigenstates as well as their complex eigenvalues for an effective non-Hermitian matrix.

We analyzed the spectra of spontaneous emission for the initial single-atom-excitation states $|D\rangle$ and $|T\rangle$ ($\equiv|T_{\mathbf{k}_I}\rangle$ with $\mathbf{k}_I = k_{eg}\hat{k}_I = k_{eg}\hat{x}$), based on vector field theory including the directions and polarizations of the wave vectors for all the vacuum modes. In the case of small volume, the timed Dicke state reduces to the standard Dicke state, which is approximately a radiative eigenmode of the system. In the intermediate-volume case, neither the standard Dicke state nor the timed Dicke state is an exponentially decaying radiative eigenmode of the system. However, nevertheless, the spectrum for $|D\rangle$ is dominated by a single peak, which is composed of multiple radiative eigenmodes with similar imaginary parts. In contrast, the spectrum for $|T\rangle$ usually has two main peaks in intermediate-volume cases, with one of them shifted to lower and one to higher frequencies by the cooperative Lamb shift. Thus, in this case, the dominating radiative eigenmodes have different eigenvalues. In very-large-volume cases, both $|D\rangle$ and $|T\rangle$ will reduce to the single-atom case without any collective effects. By separately analyzing the spectra as functions of the ensemble volume size and the number of atoms in the ensemble, we found that the structure of the spectra is predominantly determined by the system geometry. For smaller volume sizes, the system properties can be understood by analyzing the eigenvalue of a single dominant radiative eigenmode only, which as a function of the system volume size decomposes into different discrete branches. Finally, we showed that the qualitative dependence of the cooperative Lamb shift can readily be linked to the vacuum-induced dipole-dipole shift of two interacting atoms.

APPENDIX: THE EXACT FORMS OF EQ. (4)

The zeroth-order term of Hamiltonian H^S in Eq. (4) reads

$$H_0^S = \sum_{\mathbf{k}} \omega_{\mathbf{k}} b_{\mathbf{k}}^\dagger b_{\mathbf{k}} + \sum_j \sum_l \omega_l' |l\rangle_{jj} \langle l|, \quad (A1)$$

where the effective state energies are $\omega_l' = \omega_l + \delta_l$ with the single-atom nondynamic Lamb shift

$$\delta_l = -\sum_{m,\mathbf{k}} \frac{|g_{\mathbf{k},lm}|^2}{\omega_{\mathbf{k}}} \left(2\xi_{\mathbf{k},lm} - \xi_{\mathbf{k},lm}^2 + \frac{\omega_{lm}}{\omega_{\mathbf{k}}} \xi_{\mathbf{k},lm}^2 - 1 \right). \quad (A2)$$

The first-order term is

$$H_1 = \sum_{j,\mathbf{k}} \sum_{l>m} \frac{2g_{\mathbf{k},lm}|\omega_{lm}|}{\omega_{\mathbf{k}} + |\omega_{lm}|} (|l\rangle_{jj} \langle m| b_{\mathbf{k}} e^{i\mathbf{k}\cdot\mathbf{r}_j} + \text{H.c.}), \quad (A3)$$

and the second-order terms are

$$H_{V1} = -\sum_{j,\mathbf{k}} \sum_{l,m,n\neq l} \frac{g_{\mathbf{k},lm} g_{\mathbf{k},mn} \xi_{\mathbf{k},lm} \xi_{\mathbf{k},mn}}{2\omega_{\mathbf{k}}^2} |l\rangle_{jj} \langle n|$$
$$\times (2\omega_{\mathbf{k}} + 2|\omega_{lm}| + 2|\omega_{nm}| + \omega_{lm} + \omega_{nm}), \quad (A4)$$

$$H_{V2} = -\sum_{j\neq j',\mathbf{k}} \sum_{l,l',m,m'} \frac{g_{\mathbf{k},lm} g_{\mathbf{k},l'm'} \xi_{\mathbf{k},lm}}{2\omega_{\mathbf{k}}} (2 - \xi_{\mathbf{k},l'm'})$$
$$\times (e^{i\mathbf{k}\cdot\mathbf{r}_{jj'}} + \text{c.c.}) |l\rangle_{jj} \langle m| \otimes |l'\rangle_{j'j'} \langle m'|. \quad (A5)$$

[1] Z. Ficek and S. Swain, *Quantum Interference and Coherence: Theory and Experiments* (Springer, Berlin, 2005).

[2] D. A. Lidar and K. B. Whaley, in *Irreversible Quantum Dynamics*, edited by F. Benatti and R. Floreanini, Lecture Notes in Physics, Vol. 622 (Springer, Berlin, 2003), pp. 83–120.

[3] M. Kiffner, M. Macovei, J. Evers, and C. H. Keitel, in *Vacuum-Induced Processes in Multi-Level Atoms*, edited by E. Wolf, Progress in Optics, Vol. 55 (Elsevier, Amsterdam, 2010).

[4] R. H. Dicke, Phys. Rev. **93**, 99 (1954).

[5] W. Lamb and R. Retherford, Phys. Rev. **72**, 241 (1947).

[6] H. A. Bethe, Phys. Rev. **72**, 339 (1947).

[7] M. O. Scully, Phys. Rev. Lett. **102**, 143601 (2009).

[8] R. Rölsberger, K. Schlage, B. Sahoo, S. Couet, and R. Rüfer, Science **328**, 1248 (2010).

[9] J. Keaveney, A. Sargsyan, U. Krohn, I. G. Hughes, D. Sarkisyan, and C. S. Adams, Phys. Rev. Lett. **108**, 173601 (2012).

[10] R. H. Lehmberg, Phys. Rev. A **2**, 883 (1970); **2**, 889 (1970).

[11] N. E. Rehler and J. H. Eberly, Phys. Rev. A **3**, 1735 (1971).

[12] N. Skribanowitz, I. P. Hermann, J. C. MacGillivray, and M. S. Feld, Phys. Rev. Lett. **30**, 309 (1973).

[13] J. C. MacGillivray and M. S. Feld, Phys. Rev. A **14**, 1169 (1976).

[14] Y. Kagan, Hyperfine Interact. **123/124**, 83 (1999).

[15] M. O. Scully and A. A. Svidzinsky, Science **325**, 1510 (2009); **328**, 1239 (2010).

[16] A. Pálffy, C. H. Keitel, and J. Evers, Phys. Rev. Lett. **103**, 017401 (2009).

[17] M. Macovei, J. Evers, and C. H. Keitel, Phys. Rev. Lett. **91**, 233601 (2003).

[18] M. Macovei, J. Evers, and C. H. Keitel, Phys. Rev. A **71**, 033802 (2005).

[19] C. Greiner, B. Boggs, and T. W. Mossberg, Phys. Rev. Lett. **85**, 3793 (2000).

[20] F. W. Cummings, Phys. Rev. A **33**, 1683 (1986).

[21] S. Prasad and R. J. Glauber, Phys. Rev. A **61**, 063814 (2000).

[22] I. E. Mazets and G. Kurizki, J. Phys. B **40**, F105 (2007).

[23] M. O. Scully, E. S. Fry, C. H. Raymond Ooi, and K. Wódkiewicz, Phys. Rev. Lett. **96**, 010501 (2006).

[24] A. A. Svidzinsky, J.-T. Chang, and M. O. Scully, Phys. Rev. Lett. **100**, 160504 (2008); A. Svidzinsky and J.-T. Chang, Phys. Rev. A **77**, 043833 (2008), and references therein.

[25] A. A. Svidzinsky, J.-T. Chang, and M. O. Scully, Phys. Rev. A **81**, 053821 (2010).

[26] R. Friedberg and J. T. Manassah, Phys. Lett. A **372**, 2514 (2008); **374**, 1648 (2010).

[27] T. Bienaimé, N. Piovella, and R. Kaiser, Phys. Rev. Lett. **108**, 123602 (2012).

[28] Y. Li, J. Evers, H. Zheng, and S.-Y. Zhu, Phys. Rev. A **85**, 053830 (2012).

[29] J. T. Manassah, Adv. Opt. Photon. **4**, 108 (2012).

[30] H. Zheng, S.-Y. Zhu, and M. S. Zubairy, Phys. Rev. Lett. **101**, 200404 (2008).

[31] D.-w. Wang, A.-j. Li, L.-g. Wang, S.-y. Zhu, and M. S. Zubairy, Phys. Rev. A **80**, 063826 (2009); D.-W. Wang, L.-G. Wang, Z.-H. Li, and S.-Y. Zhu, *ibid.* **80**, 042101 (2009).

[32] D.-w. Wang, Z.-h. Li, H. Zheng, and S.-y. Zhu, Phys. Rev. A **81**, 043819 (2010).

[33] Z.-H. Li, D.-W. Wang, H. Zheng, S.-Y. Zhu, and M. S. Zubairy, Phys. Rev. A **80**, 023801(R) (2009); **82**, 050501 (2010).

[34] S. Yang, H. Zheng, R. Hong, S.-Y. Zhu, and M. S. Zubairy, Phys. Rev. A **81**, 052501 (2010); Q. Ai, Y. Li, H. Zheng, and C. P. Sun, *ibid.* **81**, 042116 (2010); X. Cao, Q. Ai, C. P. Sun, and F. Nori, Phys. Lett. A **376**, 349 (2012); J. Xu, S. Yang, X.-M. Hu, and M. S. Zubairy, *ibid.* **376**, 297 (2012); Y. B. Dong, Z. H. Li, Y. Li, and S.-Y. Zhu, Phys. Rev. A **85**, 013832 (2012).

[35] M. O. Scully and M. S. Zubairy, *Quantum Optics* (Cambridge University Press, Cambridge, 1997).

[36] J. P. Hannon and G. T. Trammell, Hyperfine Interact. **123/124**, 127 (1999).

[37] C. P. Sun, Y. Li, and X. F. Liu, Phys. Rev. Lett. **91**, 147903 (2003).